Bistability in thermomechanical metamaterials structured as three-dimensional composite tetrahedra

John T. Klein, Eduard G. Karpov[1]

University of Illinois at Chicago, Department of Civil and Materials Engineering, 842 W Taylor St, Chicago, IL 60607

Abstract

The letter begins with the thermomechanical model of a three degree-of-freedom tetrahedral unit cell subject to cycles of heating and cooling. Geometric nonlinearity, mechanical constraint and dissimilar material properties of thermoelastic elements lead to a build-up of thermally-driven stored strain energy as dictated by the thermomechanical potential. For certain geometric configurations and combinations of material properties in the composite structure, the solution bifurcates at a critical thermal load causing a discontinuous buckling or 'pop-through' of the interior triad. Interestingly, if the pop-through action coincides with an abrupt inward displacement of the tetrahedral vertices then the effective volume of the unit cell shrinks. The phenomenon is termed negative 'intermittent' volumetric thermal expansion. In total, six types of thermal load-response curves are identified. By systematic nonlinear analysis of the thermomechanical potential, the stability diagram and phase diagram pinpoint the locations of bifurcations, cusps and features that mark a shifts in hysteretic behavior. The diagrams map the thermomechanical response to the design of the unit cell. A region is identified in the phase diagram corresponding to the sets of design parameters that lead to the metamaterial response.

Keywords:
thermomechanical metamaterials, bistability, negative thermal expansion, thermoelasticity, geometric nonlinearity, nonlinear materials

1. Introduction

Thermomechanical metamaterials are artificially designed structures that exhibit unconventional thermomechanical behavior in response to changes in temperature [1–3]. A wide range of thermomechanical behavior is achievable by making use of multiple constituents with dissimilar material properties in composite architectures [4]. For instance, through the deliberate structuring of thermoelastic elements and proper combination of materials, it is possible to realize large positive, net zero or effective negative area or volumetric thermal expansion [5]. Thermomechanical systems capable of these properties include cellular materials [6], 2D lattices [7–10] 3D-printed lattices [11, 12], multi-phase materials [13] and origami metamaterials [14]. The first bistable thermomechanical metamaterials made use of periodically arranged superlattices to control energy dissipation in shape memory alloys [15].

In the present investigation, a bistable tetrahedral unit cell is subject to cyclic thermal loading. Bistability is a direct result of geometric nonlinearity, and features discontinuous buckling or 'pop-through' of the internal degree of freedom at a critical thermal load. External degrees of freedom, located at the tetrahedral vertices, control the effective volume of the unit cell. Because buckling in the internal degree of freedom simultaneously triggers abrupt changes in displacements in the external degrees of freedom, the buckling instability drives the discontinuous change in volume of the tetrahedron. Interestingly, metamaterial responses exhibit discontinuous contraction in the external degrees of freedom such that the effective volume of the unit cell shrinks. The structure will be shown to possess a negative effective volumetric thermal expansion over the transition.

The primary goal of this study is to provide a systematic methodology for defining geometric configurations and combinations of material properties in the design space that lead to a particular thermomechanical response. To this end, a phase diagram represents the fundamental tool that maps the response to design parameters that specify the dimensions and material properties of the unit cell [16–18]. The analysis considers thermoelastic bar elements governed by a thermally nonlinear constitutive law. Invoking these approximations leads to a simplified thermomechanical potential. The tetrahedral unit cell with an interior buckling triad represents possibly the simplest three-dimensional bistable thermomechanical structure. Use of these simplifications emphasize that the goal of the paper is to develop the basic tools for the analysis of bistable thermomechanical systems. Future studies will extend these tools to model the thermomechanics of more realistic bistable lattice systems.

Email address: ekarpov@uic.edu (Eduard G. Karpov)
[1]Corresponding author

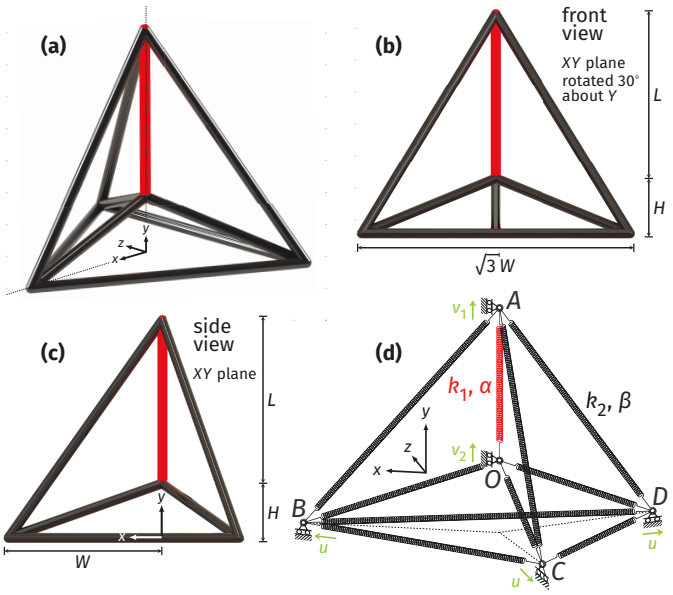

Figure 1: Thermomechanical unit cell. (a) Tetrahedron composed of ten thermoelastic bar elements. (b) Three dimensions L, H and W define the unit cell. (c) Parameter W is the distance from a vertex to the centroid of the bottom face; W is the circumradius of a regular tetrahedron. (d) Boundary conditions assume the unit cell is symmetric and positioned on a flat surface. This constrains nodes B, C and D to expand or contract in plane along the dotted lines (independent external degree of freedom u) . Due to symmetry, nodes A (external degree of freedom v_1) and O (internal degree of freedom v_2) expand or contract in the vertical direction.

2. Thermomechanical analysis

The unit cell in Figure 1 is composed of ten thermoelastic bar elements. The red middle bar has spring stiffness k_1 and coefficient of thermal expansion (CTE) α while the remaining nine black bars have k_2 and CTE β. Dimensions are defined by an initial length L of the middle bar, height H from the middle bar to the base and the tetrahedral base length $\sqrt{3}W$.

Boundary conditions model a regular tetrahedron constructed with pin-jointed truss elements and placed on a flat surface. The flat surface constrains the vertices B, C and D to move in plane along the XZ axis as depicted in Figure 1 (d). Together with the symmetry of the tetrahedron, this results in three equivalent horizontal degrees of freedom u located at these nodes. Additionally, due to symmetry the middle bar nodes O and A are constrained to move vertically along the y axis resulting in a vertical internal degree of freedom v_2 at O and vertical external degree of freedom v_1 at A. In total, there are only three independent degrees of freedom. The unit cell can be arranged periodically to form a lattice in Figure 2. The lattice material is hypothesized to maintain the properties of its constituent unit cell [11, 18].

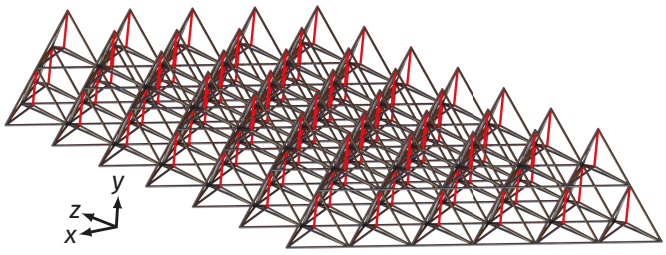

Figure 2: Thermomechanical metamaterial composed of periodic arrays of the tetrahedral unit cell.

2.1. Potential

The following definitions are used to define the thermoelastic bar problem

$$\varepsilon^T = \alpha \Delta T \qquad \text{strain due to thermal expansion} \tag{1}$$

$$\varepsilon^e = \frac{\sigma}{E} \qquad \text{elastic strain due to mechanical constraint} \tag{2}$$

$$\varepsilon = \varepsilon^e + \varepsilon^T \qquad \text{total strain} \tag{3}$$

Only the elastic component of the total strain contributes to the stored strain energy. The thermal strain is deducted from the total strain

$$\varepsilon^e = \varepsilon - \varepsilon^T \tag{4}$$

The total strain uses the Green strain definition:

$$\varepsilon = \varepsilon_G = \frac{L_f^2 - L_0^2}{2L_0^2} \tag{5}$$

The strain energy for the thermoelastic bar is

$$\pi = \frac{k}{2} L_0^2 \left(\varepsilon^e\right)^2 \tag{6a}$$

$$= \frac{k}{2} L_0^2 \left(\varepsilon_G - \varepsilon^T\right)^2 \tag{6b}$$

$$= \frac{k}{8} \frac{\left(L_f^2 - L_0^2\right)^2}{L_0^2} - \frac{k}{2} \alpha \Delta T \left(L_f^2 - L_0^2\right) + \frac{k}{2} L_0^2 \alpha^2 \Delta T^2 \tag{6c}$$

The Green strain introduces material and thermal nonlinearity into the thermomechanical potential. However, thermal nonlinearity is not essential for the buckling of the interior triad. Thermomechanical bistability is due to geometric nonlinearity rather than thermal nonlinearity. Physically, the Green strain constitutive law has the effect that if a bar is unconstrained then the rate of thermal expansion will increase as temperature is increased. This phenomenon where the magnitude of the linear coefficient of thermal expansion increases with temperature is observed in traditional materials such as metals [19] and polymers [20].

The total thermomechanical potential Π of the unit cell consists of the strain energies stored in the ten bars. The middle red bar has strain energy π_1. Strain energies π_2 in the three interior black bars are equivalent. Strain energies π_3 in the three exterior bars are equivalent. Strain energies π_4 of the three bars on the base are equivalent.

$$\Pi = \pi_1 + 3\pi_2 + 3\pi_3 + 3\pi_4 \tag{7}$$

Strain energies are found by substituting the initial and final lengths of the bars into Equation (6c)

$$\text{middle bar} \quad L_0 = L \tag{8}$$
$$L_f = L + v_1 + v_2 \tag{9}$$
$$\text{interior bars} \quad L_0 = \sqrt{W^2 + H^2} \tag{10}$$
$$L_f = \sqrt{(W+u)^2 + (H - v_2)^2} \tag{11}$$
$$\text{exterior bars} \quad L_0 = \sqrt{W^2 + (L+H)^2} \tag{12}$$
$$L_f = \sqrt{(W+u)^2 + (L+H+v_1)^2} \tag{13}$$
$$\text{base bars} \quad L_0 = \sqrt{3}W \tag{14}$$
$$L_f = \sqrt{3}W + \sqrt{3}u \tag{15}$$

2.2. Dimensionless potential

The thermomechanical potential is non-dimensionalized to reduce the number of independent system parameters. The potential is normalized by an energy term associated with the middle bar, $k_1 L^2$. The dimensionless potential U is defined

$$U = \frac{\Pi}{k_1 L^2} \tag{16}$$

Variables are redefined with dimensionless parameters. There are four system or design parameters that specify dimensions and material properties (CTE is the coefficient of thermal expansion)

$$h = \frac{H}{L} \qquad \text{ratio of distances} \tag{17}$$
$$w = \frac{W}{L} \equiv \frac{\sqrt{3}}{2} \qquad \text{ratio of distances} \tag{18}$$
$$b = \frac{\beta}{\alpha} \qquad \text{ratio of CTEs} \tag{19}$$
$$k = \frac{k_2}{k_1} \qquad \text{ratio of bar stiffnesses} \tag{20}$$

A regular tetrahedron occurs when all four faces are equilateral triangles. The unit cell is taken to be a regular tetrahedron, which fixes $w \equiv \sqrt{3}/2$. Interesting thermomechanical behavior occurs when the middle bar is softer and has a greater CTE than the other nine members, $k_1 < k_2$ or $k > 1$ and $\alpha > \beta$ or $b < 1$. This combination of material properties is physical since soft materials undergo greater thermal expansion compared to stiff materials.

Three independent state parameters determine the state of the system in space, x, y and ℓ. These are the dimensionless displacements for the three degree-of-freedom unit cell

$$x = \frac{u}{L} \qquad \text{dimensionless horizontal displacement} \tag{21}$$
$$y = \frac{v_1}{L} \qquad \text{dimensionless vertical displacement} \tag{22}$$
$$\ell = \frac{v_2}{L} \qquad \text{dimensionless internal degree of freedom} \tag{23}$$

Thus, x describes the change in width of the unit cell, y describes the change in height and ℓ describes the change in point O position, see Figure 1 (d).

The control parameter t is the dimensionless change in temperature or thermal load

$$t = \alpha \Delta T \qquad \text{dimensionless thermal load} \tag{24}$$

The coefficient of thermal expansion α is on the order of 10^{-6} to 10^{-4} K^{-1} for most engineering materials. Assuming the change in temperature ΔT is no larger than 1000 K, the thermal load t should be on the order of 0.001 to 0.1.

The dimensionless strain energies of the middle, interior, exterior and base bars

$$u_1 = \frac{1}{8}\left(y^2 + \ell^2 + 2y\ell + 2y + 2\ell\right)^2 - \frac{t}{2}\left(y^2 + \ell^2 + 2y\ell + 2y + 2\ell\right) + \frac{t^2}{2} \tag{25}$$
$$u_2 = \frac{k}{8\left(w^2 + h^2\right)}\left(x^2 + \ell^2 + 2wx - 2h\ell\right)^2 - \frac{kbt}{2}\left(x^2 + \ell^2 + 2wx - 2h\ell\right) + \frac{kb^2t^2}{2}\left(w^2 + h^2\right) \tag{26}$$
$$u_3 = \frac{k}{8\left(h^2 + w^2 + 2h + 1\right)}\left(y^2 + x^2 + 2hy + 2y + 2wx\right)^2 - \frac{kbt}{2}\left(y^2 + x^2 + 2hy + 2y + 2wx\right) + \frac{kb^2t^2}{2}\left(h^2 + w^2 + 2h + 1\right) \tag{27}$$
$$u_4 = k\left(\frac{3x^4}{8w^2} + \frac{3x^3}{2w} + \frac{3x^2}{2}\right) - kbt\left(\frac{3x^2}{2} + 3wx\right) + \frac{3k}{2}b^2t^2w^2 \tag{28}$$

The dimensionless potential becomes

$$U = u_1 + 3u_2 + 3u_3 + 3u_4 \tag{29}$$

3. Response mapping

In this section the six characteristic types of thermal load-response curves are identified and then mapped to regions in the phase diagram. The axes of the phase diagram are system parameters that specify the geometry and material properties of the unit cell. The phase diagram relates the design of the unit cell to a particular thermomechanical response. An alternative way of depicting the response is by use of a stability diagram. The stability diagram plots parametrically points of destabilization corresponding to the forward and reverse transformations of the hysteresis loop.

3.1. Thermal load-response curves

Figure 3 reveals the six distinct types of thermal load-response curves for the external degrees of freedom x and y. These degrees of freedom control the effective volume of the unit cell. Load-response of the internal degree of freedom ℓ is not plotted in Figure 3. While not shown, buckling instability in ℓ is the driving force for hysteretic bistability in the system. Load-response curves correspond to a particular design of the unit cell. Before simulating the load-response, the system or

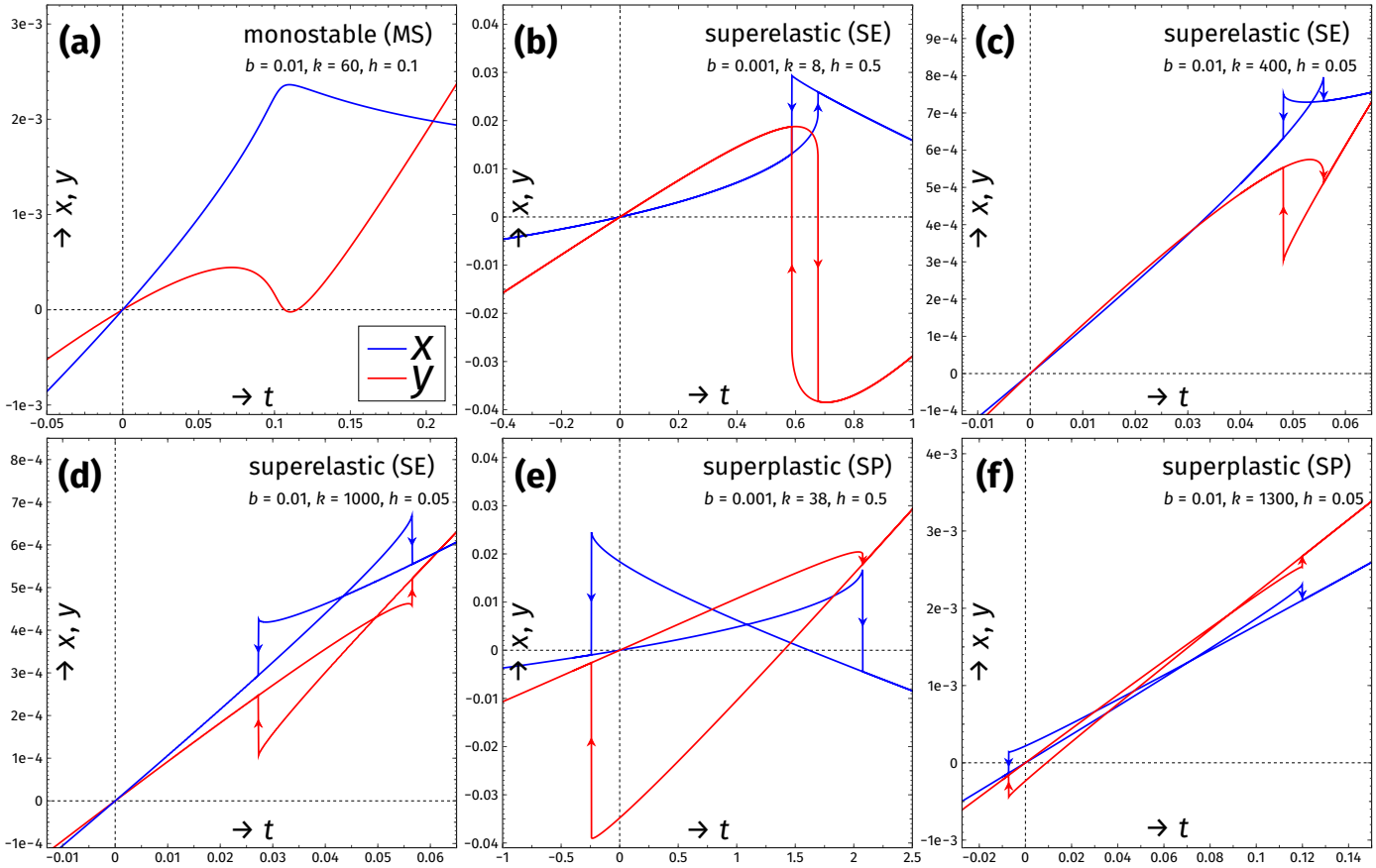

Figure 3: Six types of load-response curves for the external degrees of freedom x (blue) and y (red). The internal degree of freedom ℓ, which is the normalized displacement at node O, is not plotted. In all bistable responses, the load-response for ℓ is superelastic hysteresis due to the abrupt forward and reverse buckling events. (a) Monostable response. (b) Superelasticity with contraction in y and expansion in x at the forward transformation. (c) Superelasticity with contraction in both x and y. (d) Superelasticity with contraction in x and expansion in y. (e) Superplasticity with contraction in both x and y. (f) Superplasticity with contraction in x and expansion in y. Taking the coefficient of thermal expansion of the middle bar $\alpha = 10^{-4}$, the thermal load $t = \alpha\Delta T$ should be on the order of 0.1 when $\Delta T = 1000$ K. Thermomechanical responses (b) and (e) are unrealistic due to the large applied temperatures needed.

design parameters b, k and h are chosen. Equilibrium displacements are solved numerically for the three independent degrees of freedom x, y and ℓ using the thermal load as the running variable. To generate a complete curve, the thermal load is increased and then decreased cyclically using a small enough step size Δt. The three equilibrium conditions used to solve for the three unknown displacements at each step are

$$U'_x(b,k,h,t,x,y,\ell) = 0 \tag{30a}$$
$$U'_y(b,k,h,t,x,y,\ell) = 0 \tag{30b}$$
$$U'_\ell(b,k,h,t,x,y,\ell) = 0 \tag{30c}$$

The monostable (MS) response shown in Figure 3 (a) is characterized by smooth, continuous displacements of all degrees of freedom. For this particular set of system parameters, continuous contraction develops in y and then in x at $t \approx 0.1$. Even without bistability continuous negative thermal expansion can be realized along one or more axes of the structure. To observe the effect at reasonable temperatures, the middle bar should be fabricated of a high thermal expansion material with CTE $\alpha \approx 10^{-4}$ K^{-1}. Additionally, for this particular design the CTE of the middle bar is one hundred times as large the nine other bars, expressed by the CTE ratio $b = 0.01$. The large CTE mismatch is a tough requirement. However, as will be further discussed so long as the middle bar CTE is greater than the other nine bars ($b < 1$) the type of response does not change. A small CTE ratio b is chosen in Figure 3 (a) through (f) because it more clearly shows differences between different response types, especially what is happening with red and blue hysteresis loops in the bistable responses.

The mismatch in coefficients of thermal expansion predominately affects how much the structure displaces with changes in temperature. All else fixed, as the middle bar CTE α increases relative to the other bars β and $b = \beta/\alpha$ decreases, less displacement in the external degrees of freedom will occur for the same change in temperature.

Thermomechanical superelasticity (SE) is the first type of bistable response. The hysteresis loop is confined to positive t. As the unit cell is heated relative to the reference temperature, at the critical load it undergoes the forward transformation $A \rightarrow B$. Upon cooling, the reverse transformation $B \rightarrow A$ occurs at a lower temperature relative to the forward transformation but still above the reference temperature. The superelastic response implies the system fully recovers to its original con-

figuration when cooled back to the reference temperature.

Figure 3 (b) is the superelastic response with discontinuous contraction in y and discontinuous expansion in x. At $h = 0.5$ the interior bars meet at the tetrahedral centroid. Unrealistically large temperature excursions (> 6000 K) are required to drive the snap-through action in this particular design. It is possible to achieve this response at realistic temperature ranges by using lower h values. In the phase diagram or design space, Figure 5, the response is mapped to system parameters h and k. The response in (b) exists in the narrow region between Γ_S and Γ_x.

Figure 3 (c) is the desired superelastic metamaterial response. Both external degrees of freedom x and y undergo abrupt contraction at the forward transformation. Since the vertices of the tetrahedron are each moving inward, the structure undergoes an *intermittent negative volumetric thermal expansion*. For the x degrees of freedom, there is a 'pinched' hysteresis loop. In Section 3.4, the onset of pinched hysteresis in x is the basis for the boundary line Γ_x on the phase diagram. Γ_x is one of the two crucial boundary lines identifying sets of design parameters that lead to intermittent negative thermal expansion. Unit cells capable of this response over realistic temperature ranges possess stiffer black bars k_2 relative to the middle bar k_1. The response can be achieved over a wide range of offset parameter h, which describes the initial position of the buckling degree of freedom located at point O.

Figure 3 (d) is thermomechanical superelasticity where x contracts while y expands discontinuously. Pinched hysteresis loops exist for both external degrees of freedom. However, pinched hysteresis in y results in discontinuous upward expansion at the $A \rightarrow B$ transformation while pinched hysteresis in x results in inward contraction. The onset of pinched hysteresis in y marks the other crucial boundary Γ_y in the phase diagram. Once hysteresis in y becomes pinched, the degree of freedom loses the property of contraction at the forward transition.

The metamaterial region in the phase diagram is bounded by Γ_x and Γ_y. The region specifies unit cell dimensions and material properties that lead to intermittent contraction of both external degrees of freedom. Case (c) lies inside this region. Cases (b) and (d) fall outside this region since only one of the two external degrees of freedom experiences a critical contraction.

Thermomechanical superplasticity (SP) is the other type of bistable response. Hysteresis exists over positive and negative t. The forward transition $A \rightarrow B$ proceeds at a critical load above the reference temperature. When cooled back to the reference temperature, the structure remains deformed in state B. In order for the structure to return to its original configuration it must be cooled below the reference temperature. The reverse transformation $B \rightarrow A$ is at negative thermal load.

Figure 3 (e) is the superplastic metamaterial response. Both external degrees of freedom undergo contraction at the critical load. Designs of the unit cell that cause the superplastic metamaterial response are also within Γ_x and Γ_y on the phase diagram. However, this response is not as appealing compared to the superelastic metamaterial response in (c) since the superplastically deformed structure does not recover to its original configuration upon cooling to the reference temperature. Lastly, Figure 3 (f) is thermomechanical superplasticity where x contracts but y expands at the critical load.

3.2. Stability diagrams

The stability diagrams in Figure 4 (a) and (b) plot points of destabilization using the critical load t_c as the abscissa and a system parameter as the ordinate. Destabilization points define the onset of the forward and reverse transformations and represent bifurcations in the solution. As the control parameter is varied, the multi-surface potential evolves to create an unstable solution of equilibrium such as a saddle point. The instability leads to discontinuous jump in displacements as the solution finds a new potential well. On the stability diagrams, the right branch of the cusp-shaped curves marks the critical destabilizing load at the forward transformation while the left branch marks critical load at the reverse transformation.

The stability diagram in Figure 4 (a) fixes the stiffness ratio $k = 400$ and varies the initial offset of point O from the base h. The diagram in (b) fixes $h = 0.05$ and varies k. Plane curves are plotted in each figure for three different values of the CTE ratio b. The stability diagrams are related to the load-response. For example, find the horizontal line at $h = 0.05$ in Figure 4 (a) or $k = 400$ in (b) for the plane curve $b = 0.01$. The width between the left and right branches or difference in thermal load is identical to the width between the left and right sides of the hysteresis loop in the load-response curve in Figure 3 (c).

The sharp cusp points for each line of constant b mark the onset of bistability. The cusps always touch the same h and k value along the bottom-most dashed line, which divides monostability from bistable superelasticity. In addition, the curves of constant b all intersect $t_c = 0$ (vertical dashed line) at the same k and h values (horizontal dashed line). This second horizontal dashed line divides superelasticity from superplasticity. These two observations demonstrate that the type of response (monostability, superelasticity or superplasticity) is independent of the CTE ratio b so long as the middle bar has a greater CTE than the nine other bars. During heating, the mismatch in thermal expansion coefficients ($b = \beta/\alpha < 1$) leads to compressive strain in the middle bar and compressive strain in the other two buckling members that meet in the core. At the critical thermal load, the core buckles and releases stored strain energy, which drives the change in volume of the unit cell.

Conditions for a point on the stability diagram consist of the three equilibrium criteria and the destabilization criterion, which is defined by the 3×3 determinant of the Hessian matrix

$$U'_x(b,k,h,x,y,\ell,t) = 0 \tag{31a}$$

$$U'_y(b,k,h,x,y,\ell,t) = 0 \tag{31b}$$

$$U'_\ell(b,k,h,x,y,\ell,t) = 0 \tag{31c}$$

$$\det H(b,k,h,x,y,\ell,t) = \begin{vmatrix} U''_{xx} & U''_{xy} & U''_{x\ell} \\ U''_{yx} & U''_{yy} & U''_{y\ell} \\ U''_{\ell x} & U''_{\ell y} & U''_{\ell\ell} \end{vmatrix} = 0 \tag{31d}$$

To generate a complete stability diagram requires fixing b and either k or h, choosing a running variable such as t_c and then solving for the remaining four unknowns x, y, ℓ and either h or k using the four equations above.

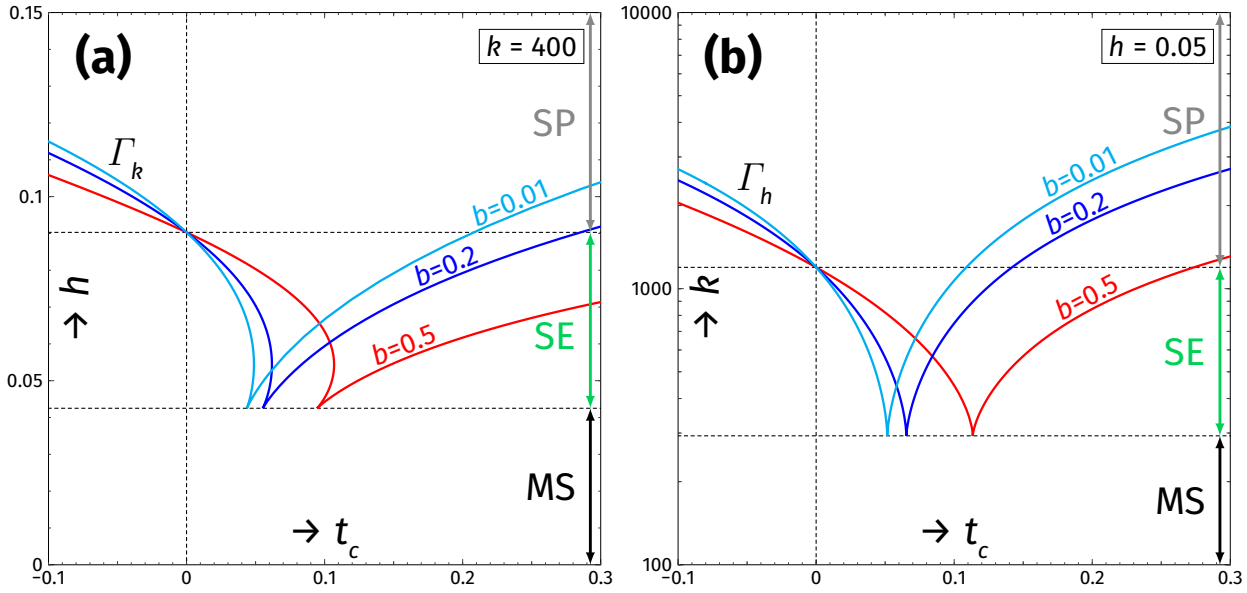

Figure 4: Stability diagrams with plane curves of constant b. The diagrams plot points of destabilization at the forward transformation (right branch of curves) and reverse transformation (left branch). (a) Stability diagram for constant $k = 400$ and varying h. (b) Stability diagram for constant $h = 0.05$ and varying k.

3.3. Numerical procedure

The Newton-Raphson root-finding method in four dimensions solves the nonlinear system, Equations (31a–31d). Known variables include two fixed system parameters and the value of the running variable at the first step. To start the method, reasonable trial solutions are guessed for the unknowns and stored in the vector $\mathbf{X}$. The system of equations is evaluated using the trial solutions and the output is stored in the residual vector $\mathbf{R}$. The Newton-Raphson method iteratively re-evaluates the vector of unknowns by taking the current iterations' unknowns $\mathbf{X}_n$ and subtracting them from the inverse of the gradient of the residual dotted with the residual, $\mathbf{X}_{n+1} = \mathbf{X}_n - [d\mathbf{R}/d\mathbf{X}]_n^{-1} \cdot \mathbf{R}_n$. The iterative loop terminates once the vector norm of the residual, $|\mathbf{R}_n| = \sqrt{\mathbf{R}_n^T \cdot \mathbf{R}_n}$, is below a specified tolerance, i.e., the converged values of the unknowns are within some precision close to the true zeros to the system of equations. To move to the next step the running variable is incremented, $t_c^{i+1} = t_c^i + \Delta t_c$, using a fine enough step size Δt_c. The Newton-Raphson method proceeds again and evaluates the unknowns at the new value of the running variable. Converged variables from the previous step are taken as the trial solutions for the current step. The process continues until enough points are generated to plot a curve.

Overall structure of the program consists of an inner Newton-Raphson loop that computes the roots to the system of equations for a single step and an outer loop that increments the running variable to transition to the next step. The end result is a set of discrete points corresponding to the four converged unknowns and value of the running variable at each step. Although the stability diagram only plots the unknown system parameter as a function of the running variable t_c, the displacements at the destabilizing thermal load are also known upon satisfying the stability conditions, Equations (31a–31d). All other systems of equations in this letter are solved using this approach, which is further discussed in [21].

3.4. Phase diagram

The six response types in Figure 3 are associated with the six regions in the phase diagram in Figure 5. The phase diagram is the design space. It maps the thermomechanical response to the design of the unit cell using design parameters h and k as the axes. Four boundary lines Γ_S, Γ_E, Γ_x and Γ_y delineate the regions. Boundary lines developed here for the analysis of thermomechanical bistable systems are analogous to those used to assess purely mechanical bistable systems [21].

The system parameters b, k and h must be specified in order to simulate the load-response. However, for this pin-jointed tetrahedron the type of response is independent of the exact choice of thermal expansion coefficients so long as the middle bar has a greater CTE than the other nine bars, see the third paragraph in Section 3.2. Once relative stiffnesses k and offset h are specified, the type of response is determined regardless of the combination of CTEs chosen. Hence, the phase diagram does not contain the parameter b since the regions of the phase diagram are functions of k and h only.

Returning to the phase diagram, the boundary line Γ_S is *the onset of bistability* and divides monostability from superelasticity. Along Γ_S are cusp singularities and solution splitting points with respect to the thermal load. When plotted on the stability diagrams in Figure 4, Γ_S points are the sharp cusps at the bottom of the beak-shaped curves. Conditions for Γ_S are based on two sets of equilibrium and destabilization criteria. The two sets are associated with either side of the hysteresis loop. Each set has different variables for the displacements x_1, y_1, ℓ_1 and x_2, y_2, ℓ_2. However, the critical load is constant across both sets, $t_1 = t_2$. At the cusp singularity the two points of destabilization on either side of the hysteresis loop meet at a single

critical load. The loop shrinks to a point. Conditions are written as

$$\Gamma_S: \quad U'_x(b,k,h,x_1,y_1,\ell_1,t_1)=0 \tag{32a}$$
$$U'_y(b,k,h,x_1,y_1,\ell_1,t_1)=0 \tag{32b}$$
$$U'_\ell(b,k,h,x_1,y_1,\ell_1,t_1)=0 \tag{32c}$$
$$\det H(b,k,h,x_1,y_1,\ell_1,t_1)=0 \tag{32d}$$
$$U'_x(b,k,h,x_2,y_2,\ell_2,t_2=t_1)=0 \tag{32e}$$
$$U'_y(b,k,h,x_2,y_2,\ell_2,t_2=t_1)=0 \tag{32f}$$
$$U'_\ell(b,k,h,x_2,y_2,\ell_2,t_2=t_1)=0 \tag{32g}$$
$$\det H(b,k,h,x_2,y_2,\ell_2,t_2=t_1)=0 \tag{32h}$$

Γ_E is the boundary between superelasticity and superplasticity. Along Γ_E the reverse transformation $B \to A$ occurs at the reference temperature, which occurs when $t = 0$. Conditions for Γ_E consist of three equilibrium equations and the destabilization criterion, setting the thermal load for the reverse transformation to zero, $t_{B\to A} = 0$

$$\Gamma_E: \quad U'_x(b,k,h,t_{B\to A}=0,x,y,\ell)=0 \tag{33a}$$
$$U'_y(b,k,h,t_{B\to A}=0,x,y,\ell)=0 \tag{33b}$$
$$U'_\ell(b,k,h,t_{B\to A}=0,x,y,\ell)=0 \tag{33c}$$
$$\det H(b,k,h,t_{B\to A}=0,x,y,\ell)=0 \tag{33d}$$

Finally, the Γ_x and Γ_y boundaries specify the onset of pinched hysteresis for the degrees of freedom x and y, respectively. This happens when a point of destabilization defined by U'_x, U'_y and U'_ℓ and $\det H$ occurs at the same critical load and critical displacement as a stable solution of equilibrium defined by U'_x, U'_y and U'_ℓ. The onset of pinched hysteresis implies the degree of freedom destabilizes and re-equilibrates at a critical load with no change in displacement. Therefore, $t_1 = t_2$ and $x_1 = x_2$ for Γ_x (or $y_1 = y_2$ for Γ_y) where x_1, y_1, ℓ_1 and t_1 are associated with a point of destabilization while the variables x_2, y_2, ℓ_2 and t_2 are associated with a stable solution of equilibrium. The conditions for Γ_x are as follows

$$\Gamma_x: \quad U'_x(b,k,h,x_1,y_1,\ell_1,t_1)=0 \tag{34a}$$
$$U'_y(b,k,h,x_1,y_1,\ell_1,t_1)=0 \tag{34b}$$
$$U'_\ell(b,k,h,x_1,y_1,\ell_1,t_1)=0 \tag{34c}$$
$$\det H(b,k,h,x_1,y_1,\ell_1,t_1)=0 \tag{34d}$$
$$U'_x(b,k,h,x_2=x_1,y_2,\ell_2,t_2=t_1)=0 \tag{34e}$$
$$U'_y(b,k,h,x_2=x_1,y_2,\ell_2,t_2=t_1)=0 \tag{34f}$$
$$U'_\ell(b,k,h,x_2=x_1,y_2,\ell_2,t_2=t_1)=0 \tag{34g}$$

The conditions for Γ_y are identical to Γ_x except $y_1 = y_2$ for the onset of pinching in y and $x_1 \neq x_2$. The region in between Γ_x and Γ_y corresponds to sets of design parameters that lead to intermittent negative volumetric thermal expansion. Load-response curves for the metamaterial behavior can be superelastic or superplastic as shown in Figure 3 (c) and (e).

4. Conclusion

This letter performs a systematic analysis of the nonlinear, non-convex thermomechanical potential governing the response of a three degree-of-freedom tetrahedral unit cell. The regular tetrahedron with a buckling core represents possibly the simplest example of a three-dimensional bistable thermomechanical system. The analysis considers only axial degrees of freedom with pin-jointed thermoelastic truss elements. The thermally nonlinear constitutive law based on the Green strain is chosen because it leads to a simple form of the thermomechanical potential. Manufacture of pin-jointed truss elements may be difficult to realize in practice. Use of other constitutive laws and inclusion of bending or rotational degrees of freedom in the thermomechanical potential may be important in capturing behavior of actual realizations. However, this does not change the fundamental approach in this paper, which is the ability to map the thermomechanical response to design parameters.

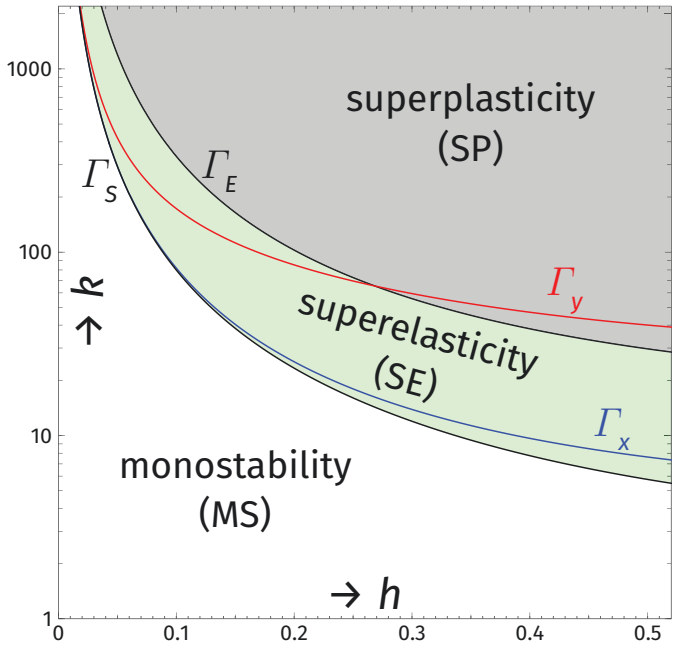

Figure 5: Phase diagram for the tetrahedral unit cell. The axes are the design parameters ($h = H/L$, $k = k_2/k_1$). Four boundary lines (Γ_S, Γ_E, Γ_x, Γ_y) define six regions. Each region is associated with a distinct 'phase' or thermomechanical response. The area between Γ_x and Γ_y defines unit cell designs with metamaterial behavior.

The analysis makes use of stability and phase diagrams, which visualize key features of the thermomechanical potential such as bifurcations, cusps and shifts in the thermomechanical response. The stability diagram operates in the control space. It plots points of instability using the critical thermal load and a single system parameter as the axes. The advantage of the stability diagram is that it depicts locations of the critical loads in bistable thermomechanical responses given specific material property combinations and unit cell configurations.

A key theoretical finding, which is visualized in the Figure 4 stability diagrams, is that the type of thermomechanical response does not depend on the CTE ratio b. Changing the CTE ratio affects the range of temperatures over which hysteresis occurs as well as the amount of initial deformation the external degrees of freedom experience before the snap-through. How-

ever, so long as the initial offset h and stiffness ratio k are specified, the thermomechanical response will be determined as one of the six basic types in Figure 3 independent of the CTE ratio.

The phase diagram is the design space. It maps the thermomechanical response to design parameters that establish the dimensions and stiffnesses of unit cell components. The phase diagram comprehensively depicts all possible thermomechanical responses across all unit cell designs. A region of negative intermittent volumetric expansion is identified between boundary lines Γ_x and Γ_y. Within this region, the buckling instability or pop-through of the internal degree of freedom drives the abrupt inward displacement of the external degrees of freedom located at the tetrahedral vertices. The phase diagram in tandem with the stability diagram provides the tools to design bistable lattice systems for a specific thermomechanical response with snap-through at a particular critically applied thermal load.

5. Acknowledgements

This work was supported by National Science Foundation via Grant #1634577.

[1] O. Sigmund, S. Torquato, Composites with extremal thermal expansion coefficients, Applied Physics Letters 69 (21) (1996) 3203–3205.
[2] L. Wu, B. Li, J. Zhou, Isotropic negative thermal expansion metamaterials, ACS applied materials & interfaces 8 (27) (2016) 17721–17727.
[3] L. Ai, X.-L. Gao, Metamaterials with negative poissons ratio and non-positive thermal expansion, Composite Structures 162 (2017) 70–84.
[4] R. Lakes, Cellular solid structures with unbounded thermal expansion, Journal of Materials Science Letters 15 (6) (1996) 475–477.
[5] G. Jefferson, T. A. Parthasarathy, R. J. Kerans, Tailorable thermal expansion hybrid structures, International Journal of Solids and Structures 46 (11-12) (2009) 2372–2387.
[6] R. Lakes, Cellular solids with tunable positive or negative thermal expansion of unbounded magnitude, Applied physics letters 90 (22) (2007) 221905.
[7] C. A. Steeves, S. L. d. S. e Lucato, M. He, E. Antinucci, J. W. Hutchinson, A. G. Evans, Concepts for structurally robust materials that combine low thermal expansion with high stiffness, Journal of the Mechanics and Physics of Solids 55 (9) (2007) 1803–1822.
[8] J. N. Grima, P. S. Farrugia, R. Gatt, V. Zammit, A system with adjustable positive or negative thermal expansion, Proceedings of the Royal Society of London A: Mathematical, Physical and Engineering Sciences 463 (2082) (2007) 1585–1596.
[9] E. Gdoutos, A. Shapiro, C. Daraio, Thin and thermally stable periodic metastructures, Experimental mechanics 53 (9) (2013) 1735–1742.
[10] N. Yamamoto, E. Gdoutos, R. Toda, V. White, H. Manohara, C. Daraio, Thin films with ultra-low thermal expansion, Advanced Materials 26 (19) (2014) 3076–3080.
[11] Q. Wang, J. A. Jackson, Q. Ge, J. B. Hopkins, C. M. Spadaccini, N. X. Fang, Lightweight mechanical metamaterials with tunable negative thermal expansion, Physical review letters 117 (17) (2016) 175901.
[12] J. Qu, M. Kadic, A. Naber, M. Wegener, Micro-structured two-component 3d metamaterials with negative thermal-expansion coefficient from positive constituents, Scientific reports 7 (2017) 40643.
[13] O. Sigmund, S. Torquato, Design of materials with extreme thermal expansion using a three-phase topology optimization method, Journal of the Mechanics and Physics of Solids 45 (6) (1997) 1037–1067.
[14] E. Boatti, N. Vasios, K. Bertoldi, Origami metamaterials for tunable thermal expansion, Advanced Materials 29 (26) (2017) 1700360.
[15] K. Guda Vishnu, A. Strachan, Shape memory metamaterials with tunable thermo-mechanical response via hetero-epitaxial integration: A molecular dynamics study, Journal of Applied Physics 113 (10) (2013) 103503.
[16] A. Rafsanjani, A. Akbarzadeh, D. Pasini, Snapping mechanical metamaterials under tension, arXiv preprint arXiv:1612.05987.
[17] L. A. Danso, E. G. Karpov, Cusp singularity-based bistability criterion for geometrically nonlinear structures, Extreme Mechanics Letters 13 (2017) 135–140.
[18] E. G. Karpov, L. A. Danso, J. T. Klein, Negative extensibility metamaterials: Occurrence and design-space topology, Physical Review E 96 (2) (2017) 023002.
[19] F. Cverna, Thermal properties of metals, ASM International, Materials Park, OH.
[20] J. E. Mark, et al., Polymer data handbook, Oxford university press New York, 2009.
[21] J. T. Klein, E. G. Karpov, Negative extensibility metamaterials: phase diagram calculation, Computational Mechanics (2017) 1–15.